The effect of stratification on tidal current profiles in a region of freshwater influence

Andre W. VISSER [a], Alejandro J. SOUZA [b], Katrin HESSNER [c] and John H. SIMPSON [b]

[a] Institute for Marine and Atmospheric Research, Utrecht University, Princetonplein 5, 3584 CC Utrecht, the Netherlands.

[b] School of Marine Sciences, University College North Wales, Menai Bridge, Anglesey LL59 5EY, United Kingdom.

[c] Institut für Meereskunde, Universität Hamburg, Troplowitzstrasse 7, D 22529 Hamburg, Germany.

ABSTRACT

Observations of the semi-diurnal tidal current ellipses within the Rhine ROFI are reported. The vertical structure of these tidal ellipses are observed to be significantly different for stratified and well mixed conditions. In particular, during well mixed conditions, tidal currents are essentially rectilinear and directed parallel to the coast. With the onset of stratification, significant cross-shore components, reaching 40% of the magnitude of the along-shore components appear. These components are 180° out of phase from near surface to near-bottom with surface currents rotating anticyclonically, and bottom currents cyclonically. It is proposed that this phenomenon may be explained by a decoupling of the upper and lower portions of the water column during stratified periods due to reduced viscosity within the pycnocline. A two layer model is used to examine this hypothesis and appears to be successful in reproducing many of the features of the observed semi-diurnal tidal ellipse variability.

RÉSUMÉ

Effet de la stratification sur le profil du courant de marée en présence de l'eau douce du Rhin

Les ellipses du courant de marée semi-diurne ont été observées en mer du Nord dans la région d'extension des eaux du Rhin. La structure de ces ellipses varie de manière significative avec la profondeur lorsqu'on passe de la stratification au mélange homogène. En particulier, dans le cas du mélange homogène, les courants de marée sont essentiellement rectilignes et orientés parallèlement à la côte. Lorsque la stratification s'établit, des composantes perpendiculaires à la côte apparaissent, pouvant atteindre 40% de l'amplitude des composantes parallèles à la côte. Ces composantes se déphasent de 180° entre la surface et le fond avec des courants anticycloniques en surface et cycloniques au fond. En régime stratifié, ce phénomène pourrait s'expliquer en distinguant les couches supérieure et inférieure de la colonne d'eau en raison de la viscosité réduite dans la pycnocline. Cette hypothèse, examinée dans le cas d'un modèle à deux couches, reproduit convenablement plusieurs caractéristiques de la variabilité observée dans l'ellipse du courant de marée semi-diurne.

Oceanologica Acta, 1994. 17, 4, 369-381.

INTRODUCTION

Recent years have seen a growing interest in the study of regions of freshwater influence (ROFI). In these regions, stratification by freshwater buoyancy input constitutes a key determinant of the environment. These regions are dynamically different from other regions of the shelf seas where seasonal stratification is present due to heating-stirring competition (Simpson and Bowers, 1984). Their parameters range between those of vertically mixed and stratified density regimes, depending on the changes in run-off and intensity of stirring. This stratification-stirring competition is relatively difficult to predict because although tidal forcing shows a regular variation in mixing rates and straining of the density field over both the spring-neap and the semi-diurnal cycles (Simpson et al., 1990), other random components, such as the variability of run-off, wind and wave stirring, as well as upwelling events (Münchow and Garvine, 1992) are involved.

The dynamics which set ROFIs apart from other regions of shelf seas are for the most part baroclinically mediated. In other words, dynamics associated with density gradients induce circulation patterns that promote the horizontal dispersion of fresh water through agencies such as coastal buoyancy currents and cross-shore "estuarine" circulation. But equally significant, perhaps, is the influence the density structure may have in modifying the water column response to dynamics that are essentially barotropic in nature. As we shall see, tidal currents appear to be a case in point.

It has long been recognized that tidal currents in shallow water exhibit a marked variation with depth. In the first place, near-surface currents are generally stronger than near-bottom currents. Furthermore, the direction of maximum tidal streaming and its rotational properties may vary from surface to bottom. Interpretation of these observed vertical variations of tidal currents has been facilitated by analyses invoking a uniform vertical eddy viscosity, e.g. Thorade 1928, Prandle 1982, Soulsby 1983. Such models explain these observations in terms of Ekman layer depth. Essentially, the component of the tide that rotates in the same direction as planetary rotation is not as strongly affected by bottom friction and has a thinner bottom Ekman layer associated with it than the component which rotates in the opposite direction, i.e. against planetary rotation.

Recent observations, e.g. Maas and van Haren 1987, Van der Giessen et al., 1990, Lwiza et al., 1991, indicate that this model fails for stratified seas. This is not altogether surprising, since vertically uniform eddy viscosity is an approximation and only credible for a homogeneous water column. With the onset of stratification, vertical motions within the pycnocline are suppressed, leading to a reduction in the scale of vertical eddies and thus to eddy viscosity over the stratified portion of the water column.

Given this relationship between stratification and vertical eddy viscosity profiles, it is possible that the vertical structure of barotrophic tidal currents may vary from time to time in response to the relative influence of stratifying and destratifying effects of variable duration. In consequence, the vertical structure of tidal currents in a variable ROFI

may vary in a systematic manner that is not well represented by a superposition of time-constant tidal constituents. This is because the dynamics governing these tidal current profiles may be non-stationary. Some factors contributing to this non-stationarity are tide-related (e.g. tidal mixing); others, such as variable wind stirring and river discharge, are non-tidal.

Here we report observations of semi-diurnal tidal ellipse profiles within the Rhine discharge plume, a ROFI in which mixed and stratified conditions periodically alternate. In order to highlight the possible influence of slowly varying stratification and viscosity, we analyse observed current records, using complex demodulation over short (one- day) sections . The resulting time series exhibit slow variations which may be presented in terms of the slow variation of the semi-diurnal tidal current ellipse. It should be stressed that such an analysis can no more than any other distinguish the dynamic origin of these slow tidal current variations, be they due to time-varying viscosity, tide-tide interactions, or to an internal tide. However, we show that these slow variations are strongly correlated to variations in stratification and the inferred viscosity regime in both time and space. Furthermore, we demonstrate that a model invoking only the viscosity effect reproduces, at least qualitatively, features of the observed slow variations. The conclusion, while not at present definitive, suggests a significant link between variations is stratification, viscosity profiles and the water column response to barotropic tidal forcing.

Rhine ROFI, October 1990

The Rhine ROFI extends northwards along the Dutch coast from the mouth of the river and to a distance of some 30 km from the coast. Inside this region (see. Fig. 1, inset), there is a residual northward flow and a vertical structure regime controlled by the competition between freshwater buoyancy and stirring processes. During October 1990, an extensive survey was carried out in this region. The survey (cf. Simpson et al., 1993), which was a co-operative effort principally between the Institut für Meereskunde, Germany (IfM), the University College of North Wales, Great Britain (UCNW), and the Netherlands Rijkswaterstaat (RWS), comprised three major elements: ship-borne hydrographic surveys; current, temperature and conductivity moorings; and HF radar measuring surface currents. It resulted in a comprehensive data set, the analysis of which is still in progress.

The mooring array of UCNW, laid out in a diamond pattern, was deployed from 23 September to 18 October 1990, (Fig. 1). Each mooring was equipped with three current meters at depths of approximately 8, 12 and 16 metres. Most of these moorings also carried temperature and conductivity sensors. The RWS moorings complemented these moorings, and were laid out along a line perpendicular to the shore at 2, 3, 5, 8, 13, and 33 km respectively from the coast along the Scheveningen (S) transect. Most of these carried two sets of current meters at about 4 m below the surface and 4 m above the sea bed respectively. At one location (the 3-km mooring), temperature and
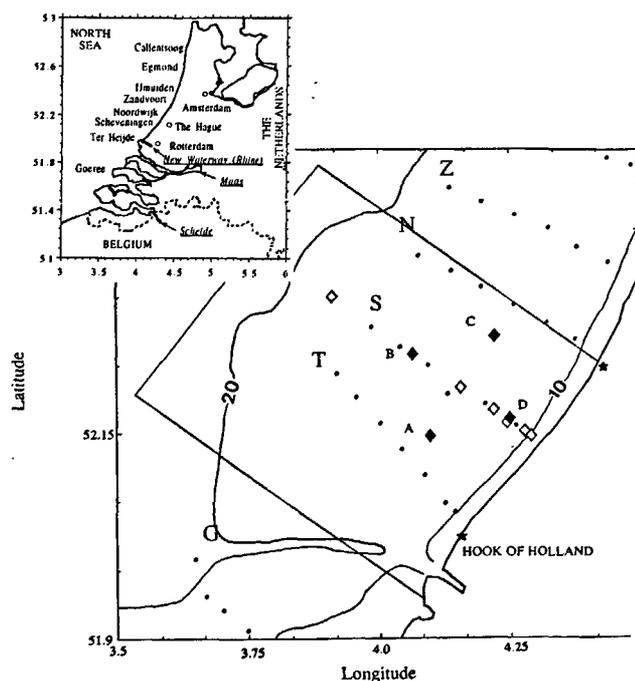
Figure 1

Netherlands coastal zone indicating the location of current and TS moorings, and the HF radar (CODAR) stations during the October 1990 integrated experiment. Ship surveys measured hydrographic parameters along shore-perpendicular transects spaced some 5 km apart from Hook of Holland to Egmont. Topography in metres. Dots represent CTD stations, diamonds mooring positions (filled diamonds UCNW, blank diamonds RWS) and stars represent the CODAR transmitters. The approximate coverage of the CODAR measurements is indicated.

conductivity sensors were placed in the upper and lower portions of the water column.

From 7 to 23 October 1990, surface currents were measured using HF radar (CODAR) with ground stations located near the Hook of Holland and Noordwijk (Fig. 1). This system is based on the principle of Doppler shift of radar echoes from waves (Barrick *et al.*, 1977) and has been successfully used in previous studies (Essen *et al.*, 1989). CODAR has a range of about 60 km with a resolution of about 2.4 km. The original CODAR data represented a 17 × 17 point grid, with a two-dimensional vector field integrated over 18 minutes and 28 km², and recorded every 30 minutes. From these data we selected the stations with more than 15 days and 300 observations so that M2 and S2 could be separated in the analysis. This reduced the grid to about 90 points roughly covering an area between 5 and 40 km from the coast and between the Ter Heijde (T) and Noordwijk (N) transects along the coast (Fig. 1).

The mooring deployments and CODAR observations were complemented by two spatial hydrographic surveys by RRS *Challenger*, one post-spring (8-10 Oct.) and one post-neap (14-16 Oct.) to observe the spatial distribution of stratification at contrasting tidal stirring regimes. This in turn was complemented by hydrographic measurements from MS *Holland* from 10 to 18 October, covering in greater detail the region between the Rhine mouth and the Noordwijk (N) transect.

Tidal currents and analysis

The tides in the southern bight of the North sea are dominated by semi-diurnal constituents, principally the M2 tide but with a significant S2 and N2 contribution. Using standard tidal analysis (Franco 1988) spanning the entire four week deployment period, we analysed the current records to obtain tidal current constituents. By way of illustration, table 1 shows the semi-diurnal tidal current constituents at two locations (3 and 13 km offshore), each for near-surface and near-bottom current measurements. In order better to visualize the rotary nature of these currents, these are presented in terms of elliptic properties, specifically the semi-major axis, ellipticity, inclination and phase (*cf.* appendix a).

It may be useful to insert here a note on ellipticity, a term that will appear frequently in what follows. A related elliptic property, eccentricity, has been used in two quite different ways in the tidal current literature. The original definition from coordinate geometry is the quantity e which relates the semi-major and semi-minor axes of the ellipse, A and B, according to:

$$e^2 = 1 - B^2 / A^2 \qquad (1)$$

while Pugh 1987 uses:

$$e = (A - B) / (A + B) \qquad (2)$$

Prandle 1982, on the other hand, follows the widely accepted practice in oceanography of defining the quantity

$$\varepsilon = B / A \qquad (3)$$

where ε varies between -1 and $+1$, with its sign determined by the sense of rotation of the ellipse (anticlockwise = cyclonic in northern hemisphere = positive). We shall follow Prandle's definition and propose that, to avoid confusion, this simple practical quantity be referred to as the "ellipticity".

Returning to the case at hand, while other tidal constituents, notably the first and second over-tides were signifi-

Table 1

Elliptic properties of the semi-diurnal tidal current components as obtained by a tidal analysis spanning the entire four-week deployment period. Inclination, Θ, is measured relative to a shore perpendicular line. These are listed for near-surface (bss = below sea surface) and near-bottom (asb = above sea bed) current meters at two locations on the Scheveningen mooring line. Total water column depth at the 3 km mooring was 16 m, and at the 13 km mooring was 19 m.

mooring location	tidal constituent	A (cm/s)	ε	Θ (deg)	φ (deg)
3 km	N2	11,85	− 0,02	95	− 83
near surface	M2	55,45	− 0,09	− 89	78
4 bss	S2	17,02	− 0,02	− 99	42
3 km	N2	8,44	0,07	97	− 80
near bottom	M2	43,67	0,09	− 89	86
4 m asb	S2	14,56	0,00	− 81	32
13 km	N2	10,26	− 0,15	98	− 64
near surface	M2	61,48	− 0,05	− 82	74
4 m bss	S2	19,68	0,00	− 90	38
13 km	N2	7,26	0,11	− 48	104
near bottom	M2	32,12	0,12	− 51	76
4 m asb	S2	12,46	0,08	46	22

cant in the analysis, they accounted for less than 10% of the variance of the semi-diurnal band. Variation of currents over the spring-neap cycle (*i.e.* M2 ± S2) is typically ±30% with respect to mean tidal conditions. Principal tidal currents are aligned parallel to the coast (*i.e.* $\Theta = \pm90°$). The ellipticity of surface M2 currents at both locations are negative near surface (ε » − 0.05 to − 0.1) (anticyclonic rotation) and positive near bottom (ε » 0.09 to 0.12) (cyclonic rotation). There is some evidence of veering with depth, particularly offshore where the near-bottom ellipse is aligned cyclonically with respect to the coastline and near-surface ellipse. Finally, in most cases these appears to be an advance in phase towards the bottom. In other words, maximum currents near the bottom occur slightly earlier than maximum currents near the surface.

It is precisely these features of tidal currents that uniform eddy viscosity models have been successful in explaining. These tidal current characteristics, however, represent to some extent a "mean" state. Specifically, in order to separate the tidal constituents, the analysis must necessarily span a long period (4 weeks). Within the Rhine ROFI over this same period, however, stratification also changes considerably, so that any influence of this on the viscosity regime and subsequent tidal current profiles has been averaged over.

To appreciate the possible influence of stratification, we might examine the current records directly. In Figure 2, for example, we present short sections of the raw current time series for spring/well mixed conditions (2 (*a*) and (*b*)), and neap/stratified conditions (2 (*c*) and (*d*)). During the spring/mixed period, the currents are dominated by a semi-diurnal oscillation in the along-shore direction and a weak cross-shore component. Furthermore, there is very little variation between near-surface and near-bottom currents. Essentially, during the spring/mixed period, the semi-diurnal current is rectilinear ($\varepsilon = 0$), directed parallel to the coast with weak vertical variation. During the neap/stratified period, however, considerably more vertical structure is in evidence. While the currents are still dominated by an along-shore semi-diurnal oscillation, a significant cross-shore component (maximum amplitude of about 35 cm/s near the surface) now appears. This cross-shore semi-diurnal oscillation appears to be ≈ 180° out of phase from surface to bottom with maximum vertical shears approaching 70 cm/s. Comparison of the phases of the across-shore and along-shore components shows anticyclonically-rotating surface currents ($\varepsilon < 0$) and cyclonically rotating bottom currents ($\varepsilon > 0$).

The development of these strong cross-shore tidal components during the neap/stratified period is particularly revealing. While a certain amount of cross-shore flow is required to fill up the beaches, (Prandle 1991), contrary to the observations this effect reaches a maximum at spring tides when the tidal prism is largest. Nor can it explain the near-bottom counter-current at neap tides. Furthermore, in order for this cross-shore velocity variation to be produced by the superposition of M2 and S2 tides, the cross-shore velocity structures associated with each of these constituents would have to be quite different, *i.e.* approximately equal in magnitude but differing in their phase relationship by approximately 180° with respect to their respective tidal
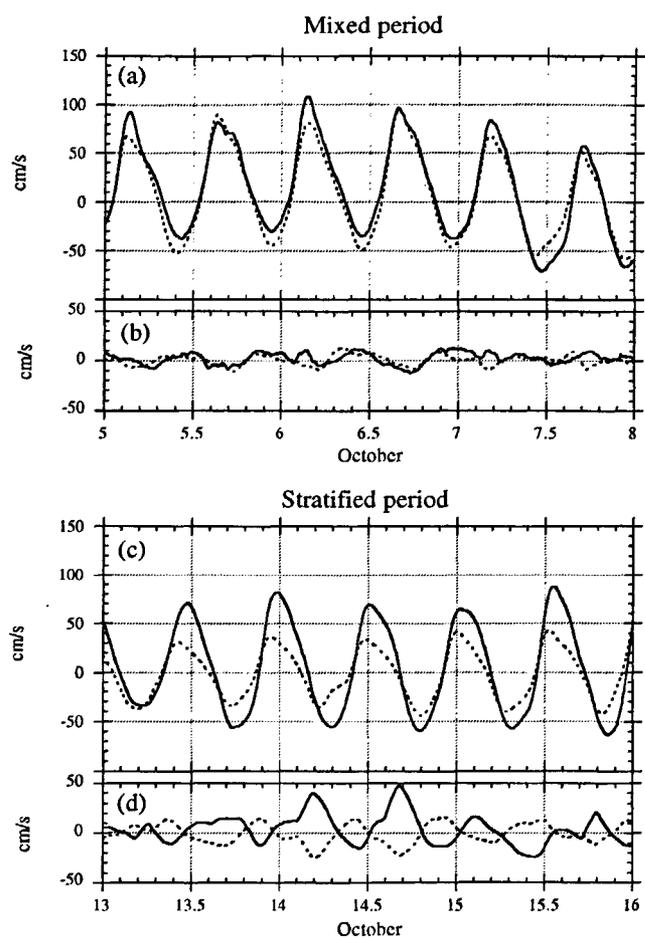
Figure 2

Time series of near-surface (solid line) and near-bottom (dotted line) along- and across-shore currents at a location 3 km off shore on the Scheveningen mooring line. (a): along-shore during well mixed period. (b): across-shore during well mixed period. (c) along-shore during stratified period. (d) across-shore during stratified period. During the well mixed period, density difference between surface and bottom was essentially 0 and during the stratified period approximately 3 kg/m³.

potentials. That is, at spring tide when M2 and S2 elevations add, their cross shore velocities subtract, and at neap tide when M2 and S2 elevations subtract, their cross-shore velocities add. This scenario is unlikely for two reasons. Firstly, due to the proximity of the coast, the vertically-integrated velocity for each constituent would have to be rectilinear and directed parallel to the coast. Any superposition would lead at all times to a coast-parallel rectilinear vertically-integrated flow. Secondly, because the same viscosity acts on each constituent and their frequencies are very nearly the same, any vertical variation induced by viscous effects would be similar, *i.e.* with very nearly the same phase relationship with respect to their respective vertically-integrated current. This suggests that the development of these cross-shore tidal currents is related to the density (and viscosity) regime, *i.e.* well mixed (= uniform viscosity) during spring tide and stratified (reduced viscosity at the pycnocline) during neap tide, rather than directly due to the superposition of the barotropic tidal waves.

In order to better quantify the variation of tidal current characteristics, we reanalysed the records using complex demo-
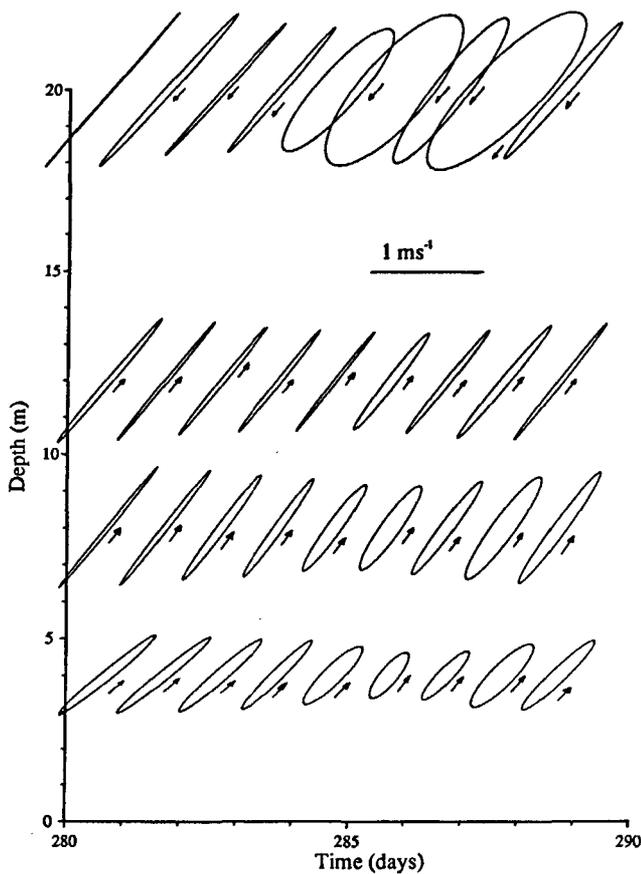
Figure 3

Vertical structure of tidal current ellipses at a location 19 km offshore on the Scheveningen (S) transect. Surface currents are from CODAR data, and subsurface from currents measured at mooring B. These cover a 10-day period marking the transition from well mixed (280 = 7 Oct) to relatively stratified conditions (290 = 17 Oct).

dulation (cf. Bloomfield, 1976). Essentially, this fits a semi-diurnal Fourier analysis to short sections ($\approx$ 1 day) of the time series (cf. appendix c). In this way, the slowly varying amplitude and phase of the semi-diurnal currents are estimated. For the RWS time series (time interval 10 minutes), a convenient semi-diurnal period was T = 12.417 hours (compared to the M2 period of 12.42 hours) and the Fourier fit was applied to successive periods of 2T. For the CODAR and UCNW time series, the time interval was 30 minutes, the semi-diurnal period was chosen as 12.5 hours with each successive fit spanning 25 hours. In practice, the analysis proved to be relatively insensitive to whichever of these semi-diurnal periods was used; both essentially remove tidal constituents outside the semi-diurnal band (i.e. MSf, O1, K1, M4, MS4, M6 etc.) while leaving the semi-diurnal constituents (i.e. M2, N2, S2, etc.) unattentuated (cf. appendix c). Of the slowly varying tidal current elliptic properties determined in this manner, only the elliptic phase has an explicit dependence on the analysis period.

RESULTS

The time and depth variation of the semi-diurnal tidal ellipse at mooring B is presented in figure 3. Within the water
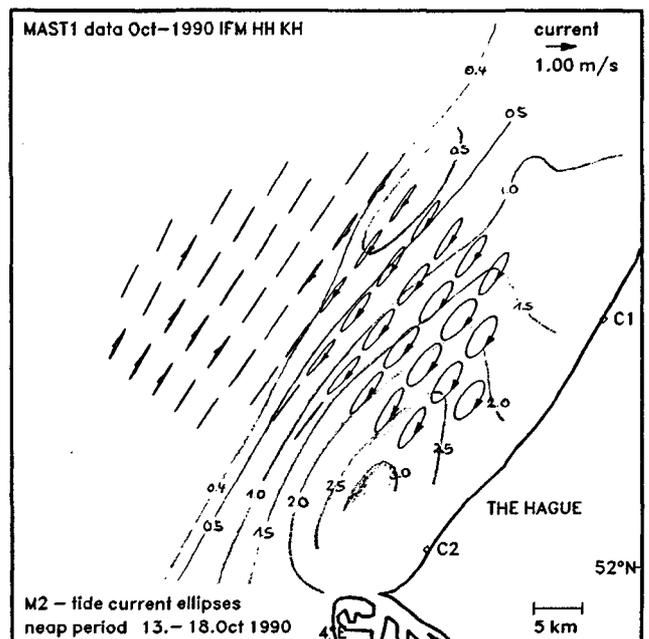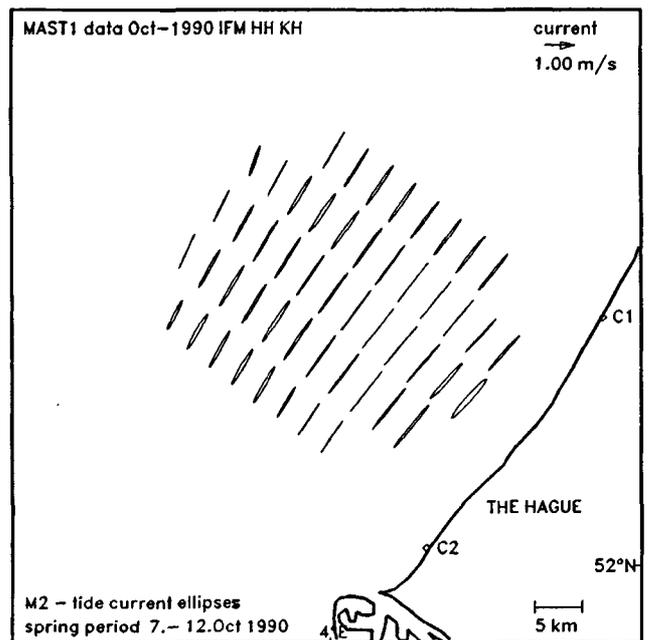
Figure 4

Surface tidal current ellipses at a few representative positions calculated from CODAR data from records for (a) spring/well mixed conditions and (b) neap/stratified conditions. These latter (b) are overlaid on a mean stratification parameter; in particular the difference in salinity between 10 m and 1 m depth constructed form an ensemble of 8 measurement campaigns between 1986 and 1989.

column, the data are from current meter records, while the surface information comes from CODAR. During well-mixed conditions (up to day 285), these show a general pattern of near-bottom cyclonic rotation decreasing with height above the sea bed, until the surface ellipses have a small anticyclonic rotation. This behaviour fits well into a homogeneous viscosity model (e.g. Prandle 1982). However, from day 285 (12 Oct.) onwards, when the water column becomes stratified, the surface tidal ellipses become strongly anticyclonic, while the lower section of the velocity profile remains cyclonic.
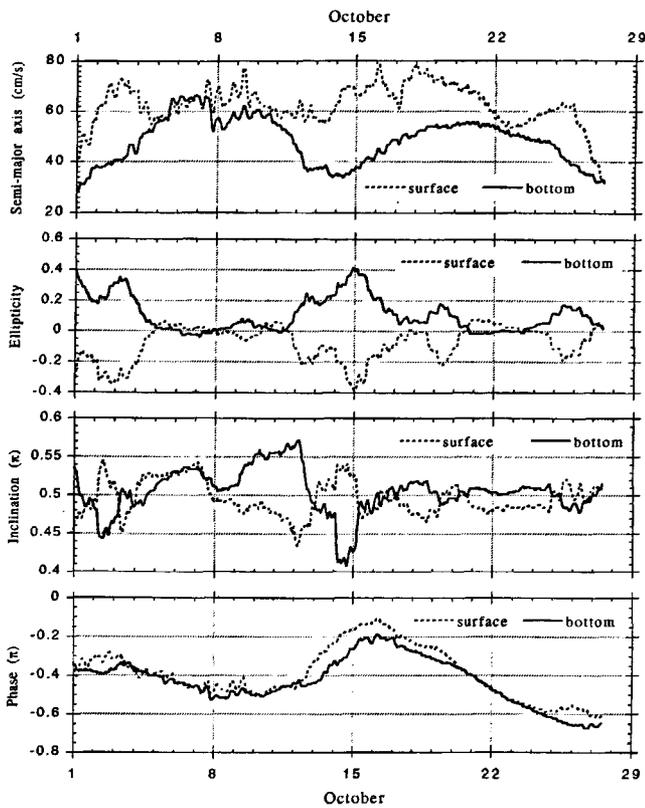
Figure 5

Low-frequency variation of tidal current ellipse properties (a): A semi-major axis, (b): ε ellipticity, (c): Θ inclination with respect to shore perpendicular line, and (d): Φ elliptic phase at a location 3 km offshore on the Scheveningen mooring line during October 1990. The surface mooring was 4 m below mean sea level, and the bottom mooring at depth 12 m. The depth of the water column at this location was 16 m. Angular measures are given in units of π radians (or 180°, or in the case of phase, 6.2 hours).

The effects of stratification can be further seen in the spatial distribution of surface semi-diurnal current ellipses. For instance, in Figure 4 we present these for spring and neap tide conditions respectively. During spring tide, (Fig. 4a), surface currents are essentially uniform and rectilinear, directed parallel to the coast. During neap tide (Fig. 4b), anticyclonic ellipticity becomes largest near the coast where stratification is generally stronger. We underscore this by superimposing a mean stratification index, specifically the difference in salinity between 10 and 1 metre depth. Where this stratification index is high, surface currents become increasingly anticyclonic (*i.e.* becomes large and negative.)

At another mooring location, 3 km offshore, the near-surface anticyclonic rotation also appeared in the moored current records. In Figure 5 we present the time series of the low-frequency variability of tidal current characteristics at 4 and 12 m depths. The spring-neap cycle is most strongly seen in the near-bottom semi-major axis. During mixed/spring conditions, both surface and bottom ellipticities are ≈ 0. With the onset of stratification (neap tide), ellipticities become large, approaching ± 0.4 with anticyclonic rotation near the surface and cyclonic rotation near the bottom. Furthermore, the inclinations of the upper and

lower axes become offset by up to 20° with respect to one another. The relative orientation of this offset appears to change sign at some point during the stratified period. Lastly, upper and lower layer ellipses are in phase during mixed periods, and become out of phase with maximum surface currents lagging behind maximum bottom currents by about 1 hour during stratified conditions. The slow modulation of the mean phase is the only significant influence of the analysis technique, which gives a slow variation at difference of the analysis and actual semi-diurnal frequencies.

Finally, in Figure 6 we compare the time variation of (a): the surface ellipticity from CODAR measurements with (b): a stratification index, (c): tidal mixing rate, and (d) and wind mixing. This demonstrates in turn the dependence of surface ellipticity on stratification, and of stratification on mixing rates. Coefficients and parameters used in determining mixing rates follow from Czitrom et al. (1988). While there may be some question as to the suitability of these for the Dutch coastal zone, we wish in the first instance to draw attention to the time variation of these mixing rates. In general, surface ellipticity follows stratification quite closely, with ε ≈ 0 for mixed conditions (until 12 Oct.) and with an abrupt transition thereafter to non-zero values. Surface ellipticity approaches a maximum of
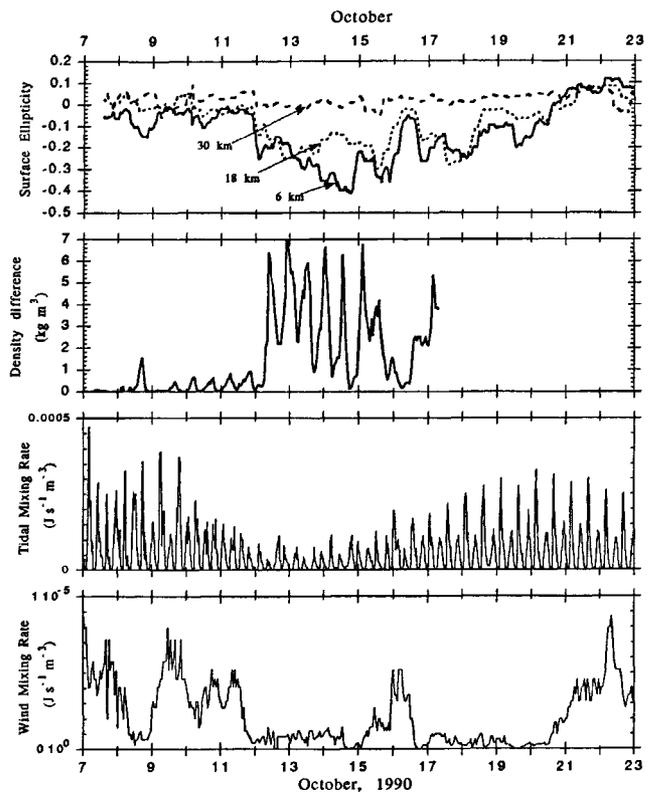
Figure 6

A comparison of the temporal variation of (a): surface current ellipticity time series from CODAR measurements at three locations, 6, 18, 30 km offshore along the Scheveningen (S) transect with (b): a stratification index, specifically the density difference between 16 and 1 below the surface at mooring A, (c): tidal mixing rate calculated from the near bottom current meter mooring 3 km offshore on the Scheveningen (S) mooring line, and (d): wind mixing rate from wind speeds measured at Noordwijk.

$\varepsilon = 0.4$ near shore during the stratified period. This effect becomes less significant further offshore where presumably stratification and hence decoupling become weaker. This correlation also extends to the "anomalous" increase of ellipticity $\varepsilon \rightarrow 0$ on 16 Oct. This may be traced back to a relatively strong wind mixing event which to some extent briefly eroded the stratification.

Interpretation

When the water column is well mixed, eddy viscosity may in the first approximation be taken as vertically uniform. In this case, some authors, e.g. Prandle 1982, Sousby 1983, predict a difference in the effective bottom Ekman layer dynamics for $U^{\pm}$ (cf. appendix a); the cyclonically rotating (+) and the anticyclonically rotating (−) components of the tide respectively. In particular, the effective Ekman layer thickness for these two components may be given by

$$\delta^{\pm} = \left\{ \frac{2\upsilon_0}{\omega \pm f} \right\}^{1/2} \tag{4}$$

where υ_0 is the eddy viscosity, ω the tidal frequency and f the Coriolis parameter. For the semi-diurnal tides (e.g. M2: $\omega = 1.41 \times 10^{-4}$ s^{-1}) in the Netherlands coastal zone ($f = 1.14 \times 10^{-4}$ s^{-1}), the ratio of these thicknesses is given by

$$\frac{\delta^+}{\delta^-} = \left\{ \frac{\omega + f}{\omega - f} \right\}^{1/2} \approx 3 \tag{5}$$

That is, the distribution of internal stresses induced by bottom drag penetrate higher into the water column for the anticyclonic rotary component than they do for the cyclonic component.

Let us suppose, by way of illustration, that we have a situation during the well mixed phase where the magnitudes of U^+ and U^- are equal at the surface, cf. Figure 7a. That is, surface tidal currents are rectilinear. With the onset of stratification (Fig. 7b), upper and lower layers become decoupled to some degree. That is, the upper layer will not feel

(a): Mixed period   (b): Stratified period
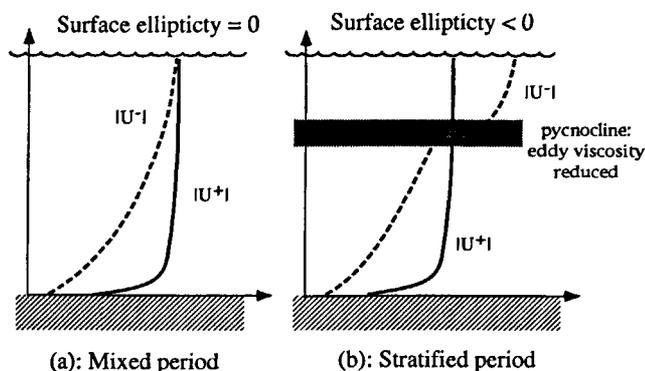
Figure 7

Conceptual sketch of the change in vertical structure of the magnitude of the cyclonic |U+| and anticyclonic |U−| rotary components of the tide for (a): well mixed, (vertically uniform υ) and (b): stratified (υ reduced in the vicinity of the pycnocline) conditions.
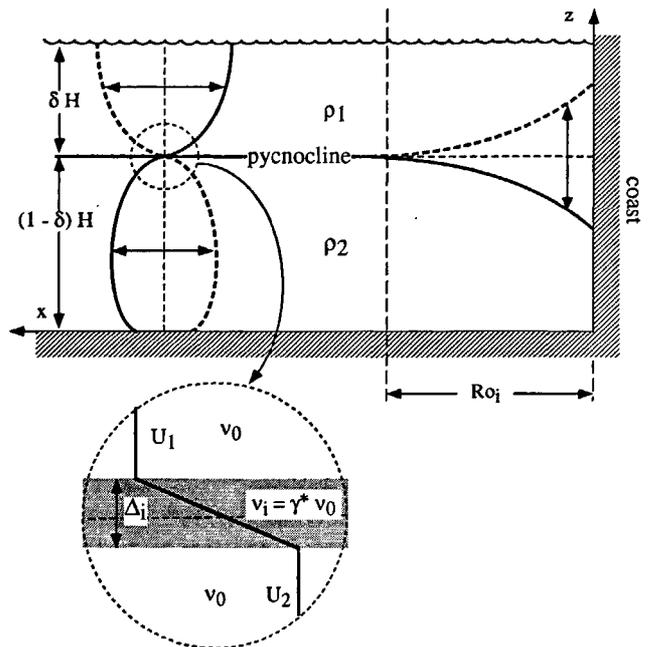
Figure 8

Sketch of the two-layer model. δ is the ratio of the upper layer thickness to total water column depth H. $U_{(1,2)}$ are the upper and lower layer cross shore velocities and are taken as vertically uniform, varying only within the vicinity of the pycnocline over a vertical distance Δ_{int}. Here, the effective viscosity becomes reduced by some factor γ.

the bottom stress as much and will move more freely in response to the barotropic forcing. With respect to the rotary components, the effect on the near surface cyclonic component will be slight, since in both cases − stratified and mixed − it is largely unaffected by bottom drag. The effect on the anticyclonic component, however, will be more dramatic, and will grow in magnitude near surface as it becomes decoupled from the lower layer.

This conceptual model consequently explains the observed increase in elliptic magnitude and anticyclonic rotation of surface currents during periods of stratification. However, it does not provide a complete explanation, as it predicts no change in the tidal current of the lower layer. With regard to this aspect, it would seem that the proximity of the coast plays an important role.

Let us consider a slightly more sophisticated model which takes this into account (Fig. 8). Suppose there is a near-surface cross-shore current directed coastwards. If a coastline is nearby, within the external Rossby radius, $Ro_e = \sqrt{gH} / f$ where g is the acceleration due to gravity and H the depth of the water column, then the net transport towards the coast must vanish with a counter-flow established in the lower layer. The upper and lower layer transports may be accommodated by a vertical deflection of the pycnocline. This deflection of the pycnocline will find place within the internal Rossby radius of deformation

$$Ro_i = \{ gH (\rho_2 - \rho_1) / \rho 2 \}^{1/2} / f$$

of the coast where ρ_1 and ρ_2 are the density of the upper and lower layers respectively. The coastal boundary condition exerts its influence on the motion over two different

spatial scales. For the water column as a whole, *i.e.* barotropically, this distance is Ro_e, which is of the order of 100 km for the Dutch coast. For the upper and lower layers individually, however, there is a "softening" of the coastal boundary constraint. The influence of the coast is not felt baroclinically beyond Ro_i from the coast. For the Rhine ROFI, this rarely exceeds 3 km.

The vertical structure of currents is determined by the manner in which momentum imparted to the fluid column by an external force, such as a pressure gradient, is redistributed by internal stresses, to be eventually lost to bottom friction. In this respect, both the bottom stress, parameterized as a linear stress law [for instance $\tau_b = k_b \mathbf{u} \, (- H)$], and internal stress, parameterized as $\tau\,(z) = - \upsilon\,(z)\,\mathbf{u}_z\,(z)$, play important roles. It turns out that bottom friction in the Dutch coastal zone is quite significant. This may be shown by relating the linearized parameter to the more commonly used quadratic stress law, namely

$$\frac{k_b}{H} \approx \frac{2}{\pi}\frac{C_D|\mathbf{U}|}{H} \approx (0.4 - 0.8) \times f \qquad (6)$$

for neap and spring conditions respectively. Here we use $C_D = 3 \times 10^{-3}$, $|\mathbf{U}| = 0.6 \pm 0.2$ m/s, and $H = 16$ m. In other words, the "spin down" time is comparable to both the tidal and inertial periods. Bulk viscosity, following Csanady 1976, may be parameterized in terms of the bottom stress as:

$$\upsilon_0 = \frac{C_D^{1/2}}{20}|\mathbf{U}|H = \frac{\pi}{40}\frac{k_b}{C_D^{1/2}}H \approx k_b H \qquad (7)$$

This parameterization is suitable for the case where the bulk Ekman layer is of the same order as or greater than the water column depth a criterion that is met in the Dutch coastal zone even at neap tides. The factor 20 is a fit parameter. Given the uncertainty in this and the drag coefficient C_D, we may reasonably take $40\,C_D^{1/2}/\pi = 1$, so that $\upsilon_0 = k_b\,H$ at least as a suitable scale.

From the homogeneous viscosity model (*cf.* appendix b), we find that relative processes determining the vertical structure of tidal currents may be written in terms of the two parameters E_0: the bulk Ekman number measuring the relative strength of internal stresses to Coriolis force, and S_0: the stress parameter (*cf.* Maas and van Haren 1987) measuring the relative strength of bottom and internal stresses. Using the above estimates of k_b and υ_0 for the Dutch coastal zone, we get $S_0=1$ and $E_0=1$ to 2 for neap to spring conditions. If we were to examine the vertical structure of the tides for the homogeneous model using these values, (*i.e.* Eq 22 in appendix b), we would find that while the magnitude of the current may vary with depth, there would be very little change in its rotary properties. In other words A decreases towards the sea bed, but neither ε, Θ nor Φ exhibit any significant vertical variation. Qualitatively, the same holds true for a layer of fluid within which the viscosity is constant and large (*i.e.* : υ_0). For the stratified case, therefore, we may model the fluid as two layers within each of which the velocity is vertically uniform and between which a certain degree of decoupling is introduced with increasing stratification. Integrating the momentum equation (Eq 19 in appendix b) within each layer, we obtain:

$$i(\omega \pm f)U_1^\pm + \frac{\upsilon_{int}}{\delta H}\frac{\partial U^\pm}{\partial z}\bigg|_{int} = P^\pm \qquad (8)$$

$$i(\omega \pm f)U_2^\pm + \frac{\upsilon_{int}}{(1-\delta)H}\frac{\partial U^\pm}{\partial z}\bigg|_{int} + \frac{k_b}{(1-\delta)H}U_2^\pm = P^\pm + G^\pm \qquad (9)$$

$$\delta HU_1^\pm + (1 - \delta)HU_2^\pm = iHU_0 / 2 \qquad (10)$$

where $U_{(1,2)}^\pm$ refer to upper and lower layers respectively, the subscript int indicates "evaluated at the interface", and δ is the ratio of the upper layer thickness to the total water column depth. The barotropic and baroclinic pressure gradients are represented by $P^\pm$ and $G^\pm$ respectively. The third equation reflects the barotropic coastal boundary constraint that at all times the vertically integrated transport in the cross-shore direction is zero. With the y (imaginary) axis aligned with the coast, this means that the vertically-integrated transport never has a real component. U_0 is the amplitude of the vertically-averaged alongshore (rectilinear) tidal current.

In order to reflect the decrease in viscosity within the pycnocline, Figure 8, we write: $\upsilon_{int} = \gamma^0\upsilon_0 = \gamma^0 k_b H$ where γ^0 ranges from 0 for complete decoupling to $= 1$ for the vertically mixed case. We may write the interfacial stress as:

$$\upsilon_{int}\frac{\partial U^\pm}{\partial z}\bigg|_{int} = \kappa_{int}fH(U_1^\pm - U_2^\pm); \quad \kappa_{int} = \frac{\upsilon_{int}}{fH\Delta_{int}} = \gamma\kappa; \quad \kappa = \frac{k_b}{fH}$$

where Δ_{int} is a measure of the thickness of the pycnocline or, in other term, the vertical scale over which significant velocity shears may appear during stratification. The modified parameter $\gamma = \gamma^0\,H/\Delta_{int}$ again indicates the degree of decoupling and includes a shear effect, *i.e.* γ increases as the shear spacing Δ_{int} decreases. Since little that is meaningful can be said about the absolute value of γ, we will simply use this to examine qualitatively variations of the dynamics with variations in coupling strength.

Using this parameterization, the vertically integrated momentum balance within each layer may be written as:

$$i(\varpi \pm 1)U_1^\pm + \frac{\kappa\gamma}{\delta}(U_1^\pm - U_2^\pm) = P^\pm / f \qquad (11)$$

$$i(\varpi \pm 1)U_2^\pm + \frac{\kappa\gamma}{1-\delta}(U_1^\pm - U_2^\pm) + \frac{\kappa}{1-\delta}U_2^\pm = (P^\pm + G^\pm) / f \qquad (12)$$

$$\delta U_1^\pm + (1 - \delta)U_2^\pm = \pm\frac{i}{2}U_0 \qquad (13)$$

where for convenience we write $\varpi = \omega / f$. Seaward of a distance Ro_i from the coast, $G^\pm$ is essentially zero, and it is this case that we focus on. Here, the equations may be readily solved to give:

$$U_1^\pm = \pm\frac{i}{2}U_0\left\{1 + \frac{\kappa\delta(1 - \delta)}{i(\varpi \pm 1)(1 - \delta)\delta + K(\gamma + \delta^2)}\right\} \qquad (14)$$

$$U_2^\pm = \pm\frac{i}{2}U_0\left\{1 + \frac{\kappa\delta^2}{i(\varpi \pm 1)(1 - \delta)\delta + K(\gamma + \delta^2)}\right\} \qquad (15)$$

In Figure 9 we show the variation of elliptic properties of the upper and lower layer tidal currents as functions of bottom drag κ and coupling strength γ. These are for the case
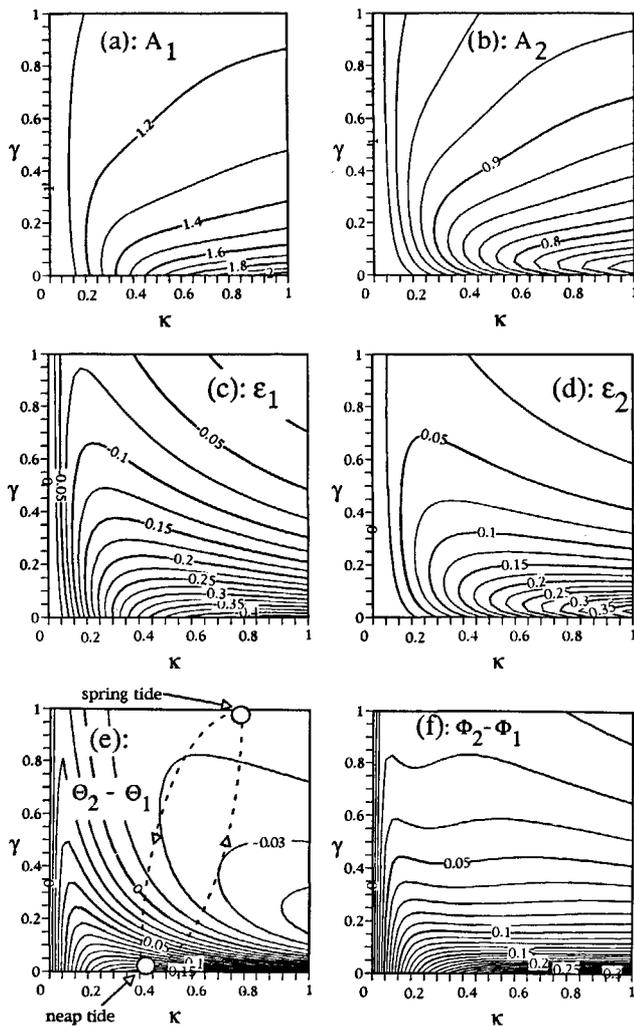
Figure 9

Elliptic properties of the surface and bottom current ellipses predicted by the decoupled two-layer model as a function of linear bottom-friction parameter κ and coupling parameter γ. Upper (a) and lower (b) layer semi-major axes; upper (c) and lower (d) layer ellipticities; relative inclination (e) and relative phase (f). Typical values of k for the Netherlands coastal zone lie between 0.4 (neap tide) and 0.8 (spring tide). The coupling parameter γ→1 for mixed conditions and γ→0 for stratified conditions The particular case presented here is for upper layer thickness δ = 0.3.

where δ = 0.3. The semi-major axes, (Fig. 9a-b) show the surface currents growing with increasing bottom drag at the expense of the bottom currents. This relative increase is moderated with an increase of viscous coupling. Note that Fig. 9a should not be interpreted as showing increasing velocities with increasing bottom drag. Rather, this effect is due to our specification that the vertically-integrated current U_0 is constant. While the orientation of this current remains constant, its magnitude will vary with varying friction and pressure gradient. In other words, Fig. 9a and b traces only the *relative* current magnitudes in upper and lower layers and cannot report anything about their absolute values. However, the ratio A_1 / A_2 for spring/mixed conditions (κ = 0.8, γ ➤ 1) and neap/stratified conditions (κ = 0.4, γ ➤ 0) gives respectively 1.2 and 1.8, which compare favourably with the observed ratios (spring/mixed = 1 to 1.2, neap/stratified=1.7) from Fig. 5a.

The ellipticity shows (Fig. 9c) surface anticyclonic rotation (ε < 0) and (Fig. 9d) bottom cyclonic rotation (ε > 0) for all κ and γ. For spring/mixed conditions (κ = 0.8, γ ➤ 1), both upper and lower layer ellipticities are small (|ε|<0.025), indicating essentially rectilinear currents throughout the water column. For neap/stratified conditions (κ = 0.4, γ ➤ 0), ellipticities approach − 0.35, and 0.2 for surface and bottom respectively. While these in general somewhat underestimate the values observed (*see* Fig. 5b), they certainly agree in rotational sense and scale.

The relative inclination of the ellipses, *i.e.* $\Delta\Theta = \Theta_2 - \Theta_1$ is shown in Fig. 9e. This is positive (*i.e.* bottom offset cyclonic with respect to surface) for small κ and γ. When both κ and γ become large, the orientation changes, so that the surface is offset anticyclonic with respect to the bottom. This behaviour is indeed exhibited in the observations, (Fig. 5c), where with the onset of stratification (*i.e.* when we may expect the bottom stress and coupling still to be relatively high), the surface-bottom offset is anticyclonic. Once stratification is well established (both bottom stress and coupling become weaker), there is a switch in orientation with the surface-bottom offset becoming cyclonic. We have sketched on Fig. 9e a conceptual trace of the spring-neap cycle in (κ,γ) space to illustrate this. The hysteresis in the curve reflects the time lag between mixing energy and response of the water column. This path passes from extreme values of $\Delta\Theta = − 2°$ (spring) to $\Delta\Theta = 27°$ (neap), crossing a local minimum, $\Delta\Theta = −4°$ to − 6°.

Finally, the relative phase Fig. 9f shows a lag between surface and bottom currents which decreases with increasing coupling strength. A maximum lag of about 1.5 hours occurs during neap/stratified conditions, somewhat higher than that observed in Fig. 5d.

In this example, (Fig. 9), we have considered the case where the upper layer occupies 30% of the total water column (δ = 0.3). Using different values of δ qualitatively leads to the same behaviour as exhibited here although the magnitude of the effect varies. The discrepancy between the values predicted in this example and those observed in reality is probably due to the variation of δ over the spring-neap cycle and the relative influences of adjustments (δ = 0.5), tidal mixing (δ decreases) and wind mixing (δ increases). A more sophisticated model, quantifying not only the viscosity/stratification relationship but also the mixing and adjustment dynamics, would be needed to take this effect into account.

DISCUSSION

Using the two-layer model, we have demonstrated that the water column response to the same periodic (semi-diurnal) barotropic forcing may be significantly different, depending on the degree of viscous coupling between the layers. Qualitatively, the dependence of viscous coupling, stratification and water column response may be seen as arising from the following effects:

• Vertical eddy viscosity is reduced during stratified periods due to a suppression of vertical eddies at the pycnocline.

This decoupling allows a significant cross-shore tidal component to develop in response to the barotropic tidal wave. Near-surface currents will exhibit an increase in anticyclonic rotation as compared to well mixed periods.

• The proximity of the coast demands that the net cross-shore tidal transport be at all times zero. This is a consequence of the barotropic boundary constraint which is in effect over a considerable distance Ro_e from the coast. This means that a near-bottom counter-current is also induced which rotates cyclonically.

• Within each layer, however, the coastal boundary constraint comes into effect only within a narrow band of width Ro_i. In effect there is a softening of the coastal boundary condition for the decoupled layer dynamics.

This view is well supported by observations. Indeed, a comparison between observations and the decoupled model show many similarities, suggesting that we have captured at least the first-order dynamics.

The effect reported here, both in observations and modelling, is not insignificant. In particular, cross-shore tidal currents with amplitudes approaching 35 cm/s appear during neap/stratified conditions. Vertical shears in these cross shore-tidal currents approach 70 cm/s, comparable with if not larger than vertical shears seen in the alongshore currents. Clearly, this may have important pragmatic implications, not the least of which relate to navigation within the busy approaches to the Rotterdam waterway and the Europort complex.

An important conclusion that might be deduced here is that in a region of freshwater influence, tidal dynamics may be non-stationary. In particular, tidal currents depend not only on tidal forcing at well defined astronomic periods, but also on the less regular and more unpredictable stratifying and destratifying processes that take place there. This begs the important question as to whether, for ROFIs, standard tidal analyses and the tidal current predictions based upon them are as robust as they might be. The same might be said of those numerical tidal models which fail to recognize the dependence of vertical viscosity profiles on stratification. Our perception of tides in ROFIs may be improved by examining the dynamics governing temporal and spatial correlations between stratification, viscosity and tidal current profiles. In the present work, albeit largely qualitative in nature, we hope to have shed some light on why this examination is important, and how it might be achieved.

Acknowledgements

Appendix A

Tidal current representation

A horizontal tidal current varying in time at a given frequency ω is fully specified by four numbers. Depending on particular applications, these may be expressed in a variety of ways, each of which are related by straightforward algebraic expressions. Most readily accessible are the amplitudes (U_a, V_a) and phases (ϕ_u, ϕ_v) of the current components (U, V) in two orthogonal directions (x, y): $U(t) = U_a \cos(\omega_t - \phi_u)$ and $V(t) = V_a \cos(\omega_t - \phi_v)$

In many instances, especially when investigating dynamics, it is convenient to combine amplitude and phase information into complex numbers (u, v): $U(t) = \text{Re}\{u \exp(-i\omega t)\}$ where $u = U_a \exp(-i\phi_u)$ and $V(t) = \text{Re}\{v \exp(-i\omega t)\}$ where $v = V_a \exp(-i\phi_v)$

Visualization of the tidal current variation with time is helped by presentation in terms of the properties of the ellipse traced out by the end-point of the vector as it rotates. These elliptic properties are: A, the semi-major axis; B, the semi-minor axis; and Θ, the inclination of A with respect to some coordinate (here, as is common we use x). ϕ is the

elliptic phase, *i.e.* $t_0 = \phi / \omega$ is the time at which the current vector achieves its maximum magnitude $(= A)$. The sign of B also defines the sense in which the vector rotates. In particular, $B > 0 \Rightarrow$ cyclonic (anticlockwise) rotation, and $B < 0 \Rightarrow$ anticyclonic (clockwise) rotation. A useful variant is ε, the ellipticity, defined as: $\varepsilon = B/A$.

While elliptic properties may be readily related to amplitudes and phases, a useful intermediate step, particularly for the analysis of dynamics, is to introduce the counter-rotating phasor representation. This is achieved by projecting the Cartesian coordinate system on to the complex Uane, with x aligned with the real, and y with the imaginary axis. The time-varying complex number representing the end-point of the current vector is then given by:

$$U(t) = U(t) + iV(t)$$

$$= \frac{1}{2}\{u\exp(i\omega t) + \tilde{u}\exp(-i\omega t)\} + \frac{1}{2}\{v\exp(i\omega t) + \tilde{v}\exp(-i\omega t)\}$$

$$= U^+ \exp(i\omega t) + U^- \exp(-i\omega t)$$

where $U^\pm = (u + iv) / 2$. Here $\sim$ indicates the complex

conjugate operation. Thus, $U(t)$ is decomposed into two constant amplitude phasors rotating in opposite directions: $U^+ \exp(i\omega t)$ in the cyclonic sense, and $\bar{U}^- \exp(-i\omega t)$ the anticyclonic sense. The maximum magnitude of $|U(t)|_{max} = A$ occurs when the counter rotating phasors are parallel. Similarly $|U(t)|_{min} = B$ occurs when they are anti-parallel. Thus $A = |U^+| + |U^-|$ and $B = A = |U^+| - |U^-|$.

Finally, writing $U^\pm = |U^\pm| \exp(i\alpha^\pm)$ leads to:

$$U(t = \Phi/\omega) = \frac{1}{2}(A+B)\exp(i(\alpha^+ + \Phi)) +$$
$$\frac{1}{2}(A - B)\exp(-i(\alpha^+ + \Phi)) = A\exp(i\Theta)$$

Solving the coefficients of A and B independently,

gives $\Theta = \frac{1}{2}(\alpha^+ - \alpha^-)$ and $\Theta = \frac{1}{2}(\alpha^+ + \alpha^-)$

APPENDIX B

Tidal current profiles for vertically uniform viscosity

Not only the tidal currents, but also the dynamics which drive them may be conveniently written in terms of counter-rotating phasors. Starting with the linearized depth dependent barotropic equations: *i.e.*

$$i(\omega \pm f)U^\pm - \{\upsilon U_z^\pm\}_z + P^\pm = 0 \tag{16}$$

$$\upsilon U_z^\pm = 0 \text{ at } z = 0 \tag{17}$$

$$\upsilon U_z^\pm = k_b U^\pm \text{ at } z = -H \tag{18}$$

where $\hat{z}$ is the unit vertical vector, f is the Coriolis parameter, H the water column depth, g the acceleration due to gravity, k_b a linearized bottom stress parameter, υ the vertical viscosity, and η the surface elevation. The boundary conditions reflect zero stress at the surface, and a matching condition of internal stress to (linear) bottom stress at the top of the bottom boundary layer. Projecting these equations on to the complex plane leads to:

$$i(\omega \pm f)U^\pm - \{\upsilon U_z^\pm\}_z + P^\pm = 0 \tag{19}$$

$$\upsilon U_z^\pm = 0 \text{ at } z = 0 \tag{20}$$

$$\upsilon U_z^\pm = k_b U^\pm \text{ at } z = -H \tag{21}$$

where $P^\pm = g(\eta_x + i\eta_y)/2$. The vertical structure of tidal currents as examined by, *e.g.* Prandle 1982, follow directly from these equations for the case where $\upsilon(z) = \upsilon_0$, *i.e.* constant with depth. In fact, these equations are then of the same form as those describing Ekman layer dynamics for a time-invariant flow from which modified solutions may be readily borrowed. Specifically

$$(z) = \frac{P^\pm}{i(\omega \pm f)} \left\{ \frac{\cosh(\beta_z^\pm / H)}{(\beta_z^\pm / S_o)\sinh(\beta^\pm) + \cosh(\beta^\pm)} - 1 \right\} \tag{22}$$

where $\beta^\pm = (1+i)\left\{\dfrac{\omega \pm f}{fE_0}\right\}$, $E_0 = \dfrac{2\upsilon_0}{fH^2}$, $S_0 = \dfrac{Hk_b}{\upsilon_0}$

and where E_0 is the bulk Ekman number, and S_0 is the stress parameter (*cf.* Maas and van Haren 1987) measuring the relative strength of bottom and internal stresses.

APPENDIX C

Semi-diurnal complex demodulation

Let us consider a prototype tidal signal of the form

$$Q(t) = \sum_n q_n \exp(i\omega_n t) \tag{23}$$

where n represents various tidal constituents, *e.g.* MSf, K1, M2, S2, N2, M4, etc. We now take the Fourier integral of this prototype tidal signal at the frequency $\omega_a = 2\pi / T_a$ over the interval $t \in [t_0 - T_a, t_0 + T_a]$.

$$Q'(t_0) = \frac{1}{2T_a} \int_{t_0-T_a}^{t_0+T_a} \sum_n q_n \exp(i(\omega_n - \omega_a)t) dt \tag{24}$$

$$= \sum_n q_n \exp(i(\omega_n - \omega_a)t_0) \frac{\sin(2\pi(\omega_n / \omega_a - 1))}{2\pi(\omega_n / \omega_a - 1)}$$

The contribution of a particular tidal constituent to $Q'(t_0)$ depends not only on its inherent amplitude q_n, but also on the attenuation function $f(\omega_n, \omega_a)$ given by

$$f(\omega_n, \omega_a) = \frac{\sin(2\pi(\omega_n / \omega_a - 1))}{2\pi(\omega_n / \omega_a - 1)} \tag{25}$$

If the analysis frequency ω_a is chosen in the semi-diurnal band, *i.e.*, T_a between 12 and 12.5 hours, then the attenuation function for the semi-diurnal constituents is ≈ 1, and for other constituents, *i.e.* diurnal, quarter-diurnal etc., is ≈ 0. This is illustrated in Figure 10 for $T_a = 12.417$, *i.e.* that chosen for the RWS time series. Very nearly identical results are obtained for $T_a = 12.5$ hours as used for the CODAR and UCNW time series. Furthermore, since for the Netherlands coastal zone the variance at any non-semi-diurnal frequency never exceeds 10% of that exhibited in the semi-diurnal band, we may to a relatively high degree of accuracy write:

$$Q'(t_0) = \exp(-i\omega_a t_0) \sum_n q_n \exp(i\omega_n t_0)$$

$$\text{for } n \in [M2, S2, N2] \tag{26}$$

This is the complex demodulated semi-diurnal tidal signal, and the tidal analysis used in this work is a numerical estimate of this procedure.
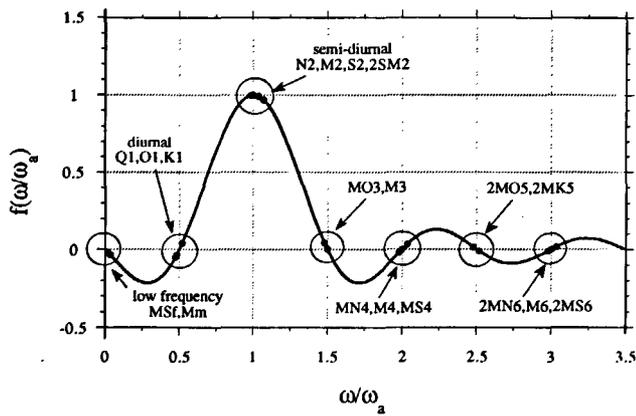
Figure 10

Now suppose we analyse tidal currents in the same manner. In terms of counter-rotating components this gives:

$$Q'(t_0) = \exp(-i\omega_a t_0)\ \{\Sigma_n U_n^\pm \exp(i\omega_n t_0)\}$$

$$\text{for } n \in [M2, S2, N2] \quad (27)$$

$$= \exp(-i\omega_a t_0)\ R^\pm(t_0) = |U^\pm(t_0)|\ \exp(i\alpha^\pm(t_0))$$

where $R^\pm$ is time-varying but independent of the analysis frequency ω_a. The elliptic properties of these current estimates may then be written as:

$$A(t_0) = \frac{1}{2}\{|R^+(t_0)| + |R^-(t_0)|\}$$

$$\varepsilon(t_0) = \{|R^+(t_0)| - |R^-(t_0)|\} / \{|R^+(t_0)| + |R^-(t_0)|\}$$

$$\Theta(t_0) = \frac{1}{2}\{\alpha^+(t_0) - \alpha^-(t_0)\} = \frac{1}{2}\arg\left\{\frac{R^+(t_0)}{R^-(t_0)}\right\}$$

$$\Phi(t_0,\omega_a) = -\frac{1}{2}\{\alpha^+(t_0) + \alpha^-(t_0)\}$$

$$= \omega_a t_0 - \frac{1}{2}\arg\left\{\frac{R^+(t_0)R^-(t_0)}{|R^+(t_0)||R^-(t_0)|}\right\}$$

That is, only elliptic phase has a specific dependence on the analysis frequency.

Finally, without going into the details here, it may be shown that for a given viscosity and bottom drag, the ratio of the rotary components for any two semi-diurnal constituents may be given by

$$r_{(n,m)}^\pm = \frac{U_n^\pm(z,t)}{U_n^\pm(z,t)} \approx \frac{\overline{U}_n^\pm}{\overline{U}_n^\pm} = \frac{\overline{A}_n}{\overline{A}_m}\exp(-i(\overline{\Phi}_n - \overline{\Phi}_m)) \quad (28)$$

This can be shown both for the vertically uniform viscosity case Eq (23) and for the two-layer model Eq (14) and (15). Here $\overline{U}_n^\pm$ represents the vertically integrated rotary components for a particular constituent with corresponding semi-major axis $\overline{A}_n$ and elliptic phase $\overline{\Phi}_n$. We have used the fact that for each constituent, the proximity of the coast requires that the vertically integrated velocity is rectilinear and directed along shore. The approximation in Eq (28) is quite robust (to about 3%) over a large range of viscosity, bottom stress and depth values and arises primarily from the small difference between the semi-diurnal frequencies. Note also that this ratio is the same for both $\pm$ components, *i.e.* $r_{(n,m)}^+ = r_{(n,m)}^-$. Assuming that the M2 constituent is dominant, then rotary components of the semi-diurnal ensemble may be written as:

$$U^\pm(t_0,z) = U_{M2}^\pm(z)\ \exp(i(\omega_{M2} - \omega_a)t_0)F(t_0)$$

$$F(t_0) = 1 + r_{(M2,S2)}\ \exp(i(\omega_{S2} - \omega_{M2})t_0)$$

$$+ r_{(M2,N2)}\ \exp(i(\omega_{N2} - \omega_{M2})t0)$$

which leads to the following elliptic properties for the complex demodulated semi-diurnal currents:

$$A(t_0) = A_{M2}(z)\ |F(t_0)|$$

$$\varepsilon(t_0) = \varepsilon_{M2}(z)$$

$$\Theta(t_0) = \Theta_{M2}(z)$$

$$\Phi(t_0) = \Phi_{M2}(z) + \omega_a t_0 - \arg\{F(t_0)^2 / |F(t_0)|^2\} / 2$$

If the tidal dynamics are stationary, that is to say if the tidal response can be well represented by the superposition of time-invariant tidal constituents, then the complex demodulated semi-diurnal current ellipse would exhibit no time variation in ellipticity or inclination. On the other hand, if time variations in these two elliptic properties are observed (as reported in this work), then non-stationary tidal dynamics, *e.g.* time-varying viscosity, play an important role.

REFERENCES

Barrick, D.E., M.W. Evans, and B.L. Weber (1977). Ocean surface currents mapped by radar. *Science*, **198**, 138-144.

Bloomfield, P. (1976). *Fourier Analysis of Time Series: An Introduction*, John Wiley and Sons, New York, 258 p.

Czitrom, S.P.R., G. Budeus and G. Krause (1988). A tidal mixing front in an area influenced by land runoff. *Cont. Shelf Res.*, **8**, 225-237.

Csanady, G.T. (1976). Mean circulation in shallow seas. *J. Geophys. Res.*, **81**, 5389-5399.

Essen, H.H., K.W. Gurgel and F. Schirmer (1989). Surface currents int the Norvegian Channel measured by radar in March 1985. *Tellus*, **41**, 162-174.

Franco A.S. (1988). *Tides: Fundamental Analysis and Prediction*. Fundaçao Centro Tecnológico de Hidráulica, Sao Paulo. 249 p.

Giessen, A. van der, W.P.M. de Ruijter and J.C. Borst (1990). Three dimensional current structure in the Dutch coastal zone. *Neth. J. Sea Res.*, **25**, 45-55.

Lwiza, K.M.M., D.G. Bowers and J.H. Simpson (1992). Residual and tidal flow at a tidal mixing front in the North Sea. *Cont. Shelf Res.*, **11**, 1379-1395.

Maas, L.R.M. and J.J.M. van Haren (1987). Observations on the vertical structure of tidal and inertial currents in the central North Sea. *J. Mar. Res.*, **45**, 293-318.

Münchow A. and R.W. Garvine (1993). Buoyancy and wind forcing of a coastal current. *J. Mar. Res.*, **51**, 293-322.

Prandle, D. (1982). The vertical structure of tidal currents. *Geophys. Astrophys. Fluid Dyn.*, **22**, 29-49.

Prandle, D. (1991). *Prog Oceanogr.*, **27**, 403-438.

Pugh, D.T. (1987). *Tides, Surges and Mean-Sea Level.* John Wiley and Sons, New York. 472 p.

Simpson, J.H., J. Brown, J. Matthews, and G. Allen (1990). Tidal straining, density currents and stirring in the control of estuarine stratification. *Estuaries*, **13**, 125-132.

Simpson, J.H., W.G. Bos, F. Schirmer, A.J. Souza, T.P. Rippeth, S.E. Jones and D. Hydes (1993). Periodic stratification of the Rhine ROFI in the North Sea. *Oceanologica Acta*, **16**, 23-32.

Simpson, J.H. and D.G. Bowers (1984). The role of tidal stirring in controlling the seasonal heat cycle in shelf areas. *Annls. Geophys.*, **2**, 411-416

Soulsby, R.L. (1983). *The bottom boundary layer of shelf seas.* in *Physical Oceanography of Coastal and Shelf Seas*, (ed. B. Johns), Elsevier, 189-266.

Thorade, H. (1928). Gezeitenuntersuchungen in der Deutschen Bucht der Nord*see*. *Deutsche Seewarte*, **46**, No. 3. Hamburg. 85 p.